

Multielement statistical evidence for uraniferous hydrothermal activity in sandstones overlying the Phoenix uranium deposit, Athabasca Basin, Canada

Shishi Chen¹  · Keiko Hattori¹ · Eric C Grunsky²

Received: 26 October 2015 / Accepted: 27 June 2017 / Published online: 8 July 2017
© Springer-Verlag GmbH Germany 2017

Abstract The Phoenix U deposit, with indicated resources of 70.2 M lb U₃O₈, occurs along the unconformity between the Proterozoic Athabasca Group sandstones and the crystalline basement rocks. Principal component analysis (PCA) is applied to the compositions of sandstones overlying the deposit. Among PCs, PC1 accounts for the largest variability of U and shows a positive association of U with rare earth elements (REEs) + Y + Cu + B + Na + Mg + Ni + Be. The evidence suggests that U was dispersed into sandstones together with these elements during the uraniferous hydrothermal activity. Uranium shows an inverse association with Zr, Hf, Th, Fe, and Ti. Since they are common in detrital heavy minerals, such heavy minerals are not the major host of U. The elements positively associated with U are high in concentrations above the deposit, forming a “chimney-like” or “hump-like” distribution in a vertical section. Their enrichment patterns are explained by the ascent of basement fluids through faults to sandstones and the circulation of basinal fluids around the deposit. The Pb isotope compositions of whole rocks are similar to expected values calculated from the concentrations of U, Th, and Pb except for sandstones close to the deposit. The data suggest that in situ decay of U and Th is responsible for

the Pb isotope compositions of most sandstones and that highly radiogenic Pb dispersed from the deposit to the proximal sandstones long after the mineralization. This secondary dispersion is captured in PC8, which has low eigenvalue. The data suggests that the secondary dispersion has minor effect on the overall lithochemistry of sandstones.

Keywords Lithochemistry · Principal component analysis · Unconformity-type uranium deposits · Hydrothermal alteration · Multivariate statistical analysis

Introduction

The Athabasca Basin is a large Proterozoic sandstone basin located in northern Saskatchewan and Alberta, Canada (Fig. 1). This basin hosts the world’s largest high-grade U resources along the unconformity between the sandstones and underlying crystalline basement rocks (Hoeve and Sibbald 1978; Jefferson et al. 2007). These U deposits are accompanied by alteration halos, which overprint the diagenetic minerals of sandstones and the metamorphic minerals of the basement rocks (Hoeve and Quirt 1984; Kotzer and Kyser 1995). The alteration halos commonly extend several hundred meters around major deposits (Hoeve and Quirt 1984; Kotzer and Kyser 1995; Kister et al. 2006), and alteration minerals include illite, kaolinite, dravitic tourmaline, aluminum phosphate sulfate (APS) minerals, and Mg-chlorite (Hoeve and Quirt 1984; Quirt et al. 1991; Quirt and Wasyluk 1997; Jefferson et al. 2007). The alteration resulted in significant changes in lithochemistry of sandstones. For example, increased K/Al ratios due to illitization of sandstones above the Midwest U deposit are reported (Sopuck et al. 1983), and anomalously high contents of Na, Sr, Y, Pb, Th, As, and P occur above the Cigar Lake deposit and the Dawn Lake mineralized zones (Clark 1987). Enrichment of elements associated

Editorial handling: M. Fayek

Electronic supplementary material The online version of this article (doi:10.1007/s00126-017-0756-2) contains supplementary material, which is available to authorized users.

✉ Shishi Chen
schen162@uottawa.ca

¹ Department of Earth and Environmental Sciences, University of Ottawa, 25 Templeton Street, Ottawa, ON K1N 6N5, Canada

² Department of Earth and Environmental Sciences, University of Waterloo, 200 University Ave. W, Waterloo, ON N2L 3G1, Canada

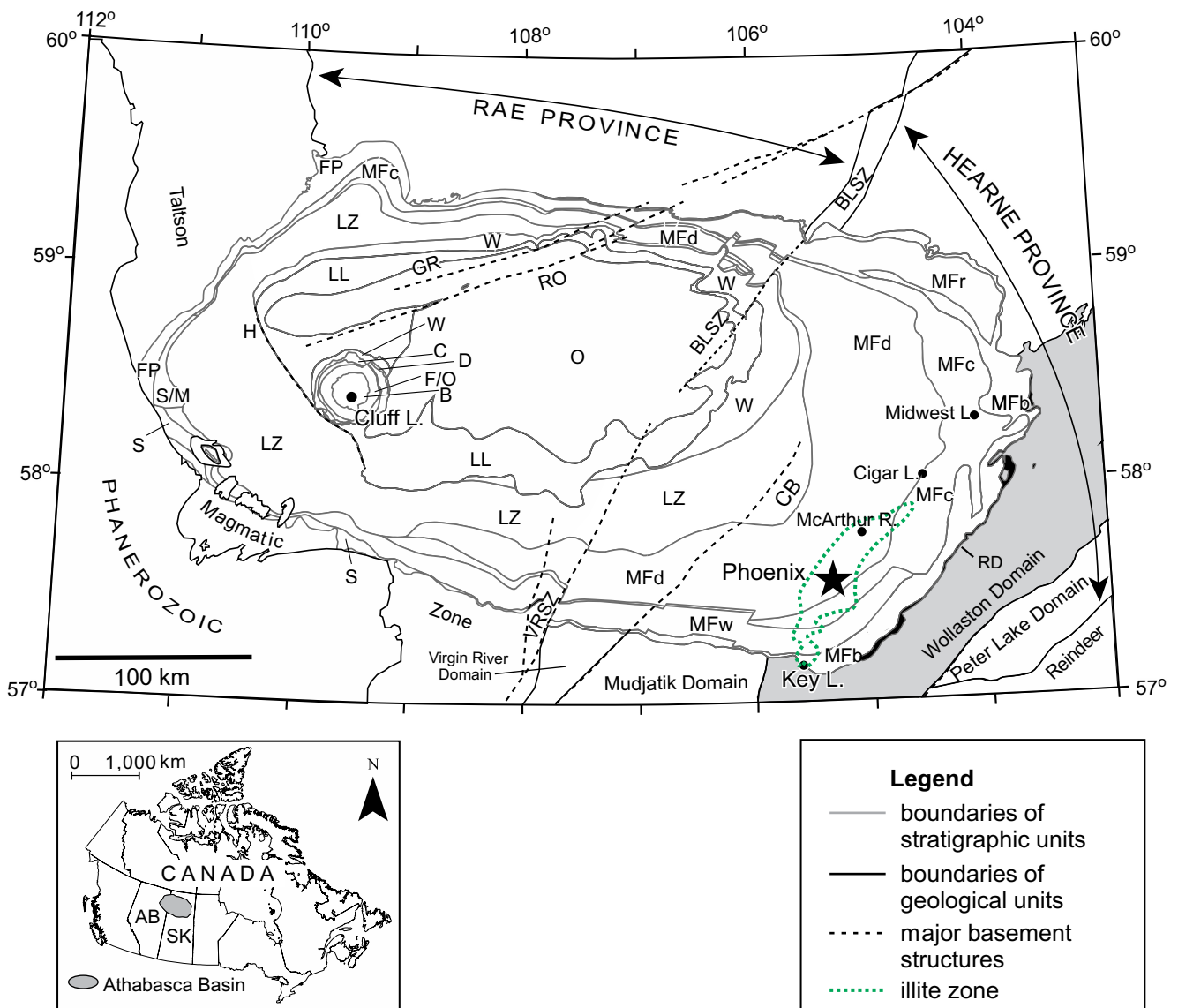


Fig. 1 Simplified geological map of the Athabasca Basin (after Jefferson et al. 2007) and the locations of selected major U deposits (solid circles). The Phoenix deposit (solid star) is underlain by the basement rocks of the Wollaston Domain (shaded area) close to the contact with the Mudjalik Domain. Major shear zones: Black Lake Shear Zone (BLSZ), Cable Bay (CB), Grease River Shear Zone (GR), Harrison Shear Zone (H), Robbilar (RO), Virgin River Shear Zone (VRSZ). Formations: basement (B), Fair Point Formation (FP), Smart Formation (S), undifferentiated

Smart and/or Manitou Falls (S/M), Read Formation (RD), Manitou Falls Formation (MF; Bird Member (b), Warnes Member (w), Collins Member (c), Dunlop Member (d)), Lazenby Lake Formation (LZ), Wolverine Point Formation (W), Locker Lake Formation (LL), Otherside Formation (O), Douglas Formation (D), Carswell (C), undivided Fair Point to Otherside Formations (F/O). The inserted map shows the location of the Athabasca Basin. AB province of Alberta, SK province of Saskatchewan

with U deposits is also reported in sandstones near several other U deposits (Mellinger et al. 1987; Dann et al. 2014; Wright et al. 2015; Guffey et al. 2015). These previous studies used univariate and bivariate methods to show the variations in abundance of individual elements, but associations of these elements have not been evaluated.

Significant U deposits in Athabasca Basin, including the McArthur River and Cigar Lake deposits, are located in the

eastern part of the Athabasca Basin (Fig. 1). The Phoenix deposit is one of such unconformity-related U deposits in the eastern Athabasca Basin and estimated to contain indicated resources of 70.2 M lb U_3O_8 at a grade of 19.1% U_3O_8 (Roscoe 2015). More importantly, it is the highest tonnage, undeveloped U deposit in the basin (Roscoe 2015).

Geochemical data are commonly assessed by univariate and bivariate methods. Univariate methods commonly use

histograms, quantile-quantile plot, box-and-whisker plot, etc. Bivariate methods (e.g., correlation matrix) show the relationship between two variables but are not able to observe multivariate associations. Aitchison (1986) and Filzmoser et al. (2010) demonstrated that compositional data are not represented in the standard Euclidean space and that bivariate analysis may lead biased results. Multivariate analysis after appropriate transformation of geochemical data can show unbiased linear relationship of elements (Grunsky 2010; Filzmoser et al. 2010).

In order to quantitatively identify the elements associated with U in sandstones, R-Q (R = variables, Q = observations) mode PCA, a multivariate statistical technique, is employed. This method reduces dimensionality of a data set to observe the linear relationship of the variables. This paper reports the result of the statistical analysis of lithogeochemical data, evaluates the minerals responsible for element associations, and discusses the geological process leading to the element distribution in sandstones.

Study area and samples

Geological setting of the Athabasca Basin

The Athabasca Basin occupies much of the northernmost quarter of Saskatchewan and extends to the west into northern Alberta in Canada (Fig. 1). The rocks of the basin deposited in several sub-basins and are composed of quartz arenite and quartz-pebble conglomerate of dominantly fluvial to shallow marine origin of Athabasca Group sedimentary rocks with the current maximum thickness of 1500 m in the center of the Basin (Ramaekers et al. 2007). The basal formation in the eastern part of the basin is the Read Formation (RD), which is composed of quartz arenite, quartz-pebble conglomerate, and lenses of red silty mudstone. The Manitou Falls (MF) Formation is divided into the Bird Member (MFb), Collins Member (MFc), and Dunlop Member (MFd) in ascending order. These units show overall upward-fining succession of quartz arenite, planar and trough cross-bedded quartz arenite, minor horizontally bedded quartz arenite, and thinly bedded, fine-grained sandstones to mudstones with interbedded quartz-pebble conglomerate. The MFd is the uppermost unit in the eastern part of the basin (Fig. 1). The Athabasca Basin development likely ended at around 1540 Ma, which is the age of the uppermost Douglas Formation in the western part of the basin (Creaser and Stasiuk 2007). Diagenesis resulted in silica cementation on hematite-dusted detrital quartz grains (Hoeve and Sibbald 1978; Jefferson et al. 2007), followed by the transformation of kaolinite to dickite (Laverret et al. 2006) and partial conversion of kaolinite to illite (Hoeve and Quirt 1984).

The basement rocks in the eastern basin belong to the Wollaston Domain of the Hearne Province and comprise Paleoproterozoic metasedimentary rocks overlying Archean granites (Fig. 1). The highly deformed rocks of the Wollaston Group consist of metapelitic, psammitic, arkosic, calc-silicate gneisses, quartzite, and lenses and dykes of anatectic granitic pegmatites (Annesley et al. 2005; Yeo and Delaney 2007). They were metamorphosed under upper amphibolite to lower granulite facies conditions during the Trans-Hudson Orogeny, ca. 1.8–1.9 Ga (Lewry and Sibbald 1980; McKechnie et al. 2012). The basement rocks contain numerous reverse faults along graphitic beds and along lithological boundaries between quartzite and pelitic rocks. These faults were repeatedly reactivated to offset the unconformity between the sandstones and basement locally on the order of tens of meters and were important in controlling the deposition of sandstones (McGill et al. 1993; Ramaekers et al. 2007) and hydrothermal fluid flow (Hoeve and Quirt 1984; Li et al. 2015).

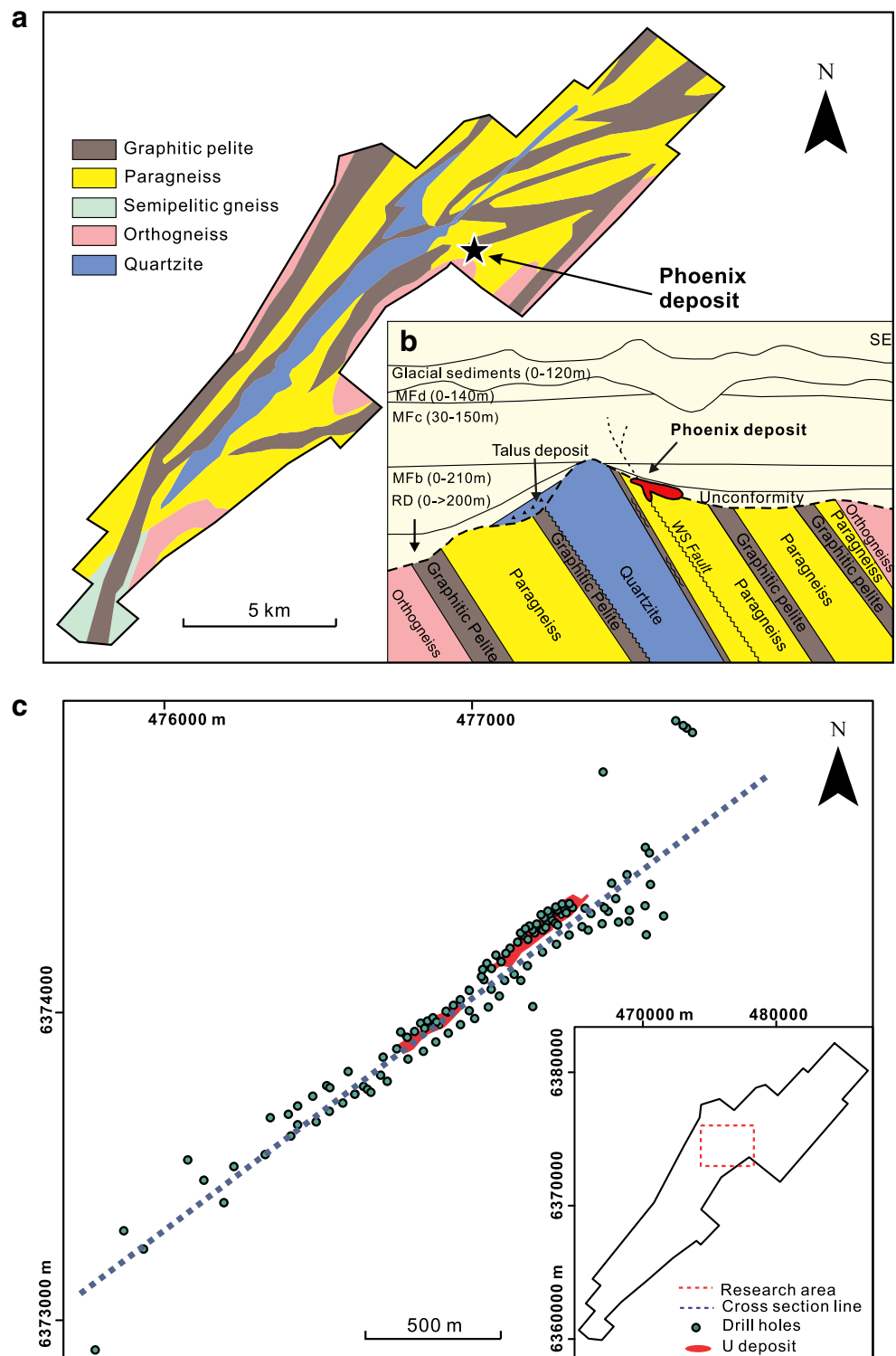
It is generally considered that oxidizing uraniferous fluids are reduced by basement-derived fluids to precipitate U along the unconformity (Hoeve and Sibbald 1978; Hoeve and Quirt 1984; Fayek and Kyser 1997; Quirt 2003; Jefferson et al. 2007). All known U deposits occur in the proximity of basement faults, suggesting that faults likely acted as conduits for the basement fluids to reach the unconformity (Hoeve and Sibbald 1978; Hoeve and Quirt 1984; Wallis et al. 1984; McGill et al. 1993). A study of alteration minerals in and around the McArthur River deposit by Adlakha and Hattori (2015, 2016) supports the important role of basement faults as conduits of basinal and basement fluids.

In the southeastern portion of the basin, occurrence of illite in the uppermost sandstones form a zone of regional illite alteration, ~25 km in width, extends from the Key Lake deposit to past the McArthur River deposit (Fig. 1), and this illite zone envelops Mg-chlorite and dravitic tourmaline zones (Earle and Sopuck 1989). The study area is within these regional alteration zones (Fig. 1).

Study area

The Athabasca sandstones in the study area are around 400 m in thickness, but are thin, ~200 m, above quartzite ridges (Fig. 2a, b). Quartzite became an erosional remnant during the weathering of the basement rocks and remained as ridges during the deposition of sandstones (Fig. 2a). The sandstone units at the Phoenix deposit consist of the Read Formation and three members of MF described in the previous section. At the Phoenix deposit, the MFb is distinguished from the underlying RD and overlying MFc by the presence of at least 1 to 2 vol% conglomerate beds. This member also contains heavy-mineral seams. The MFc is composed of relatively clean

Fig. 2 **a** Basement geological map of the Phoenix deposit area at the unconformity (after Roscoe 2015). **b** NW-SE cross section of the Phoenix deposit (modified after Gamelin et al. 2010). Paragneiss contains graphitic layers. **c** Schematic map showing the drill hole collar locations used in this study. The red dashed line shows the area containing the samples used in this study. The blue dashed line represents the location of the section used in Figs. 4c, 5b, 6c, 7c, and 8d. Note that background drill hole WR-367 is not shown in this map as it is located ~3 km southwest of the deposit. The samples from the drill hole, WR-367, show no significant concentrations of U, (HREE + Y), B, MgO, and Fe₂O₃ and low ratios of ²⁰⁶Pb/²⁰⁴Pb



quartz arenite with locally scattered granules or pebbles, whereas the MFd is distinguished from the underlying MFC by the presence of abundant (>1 vol%) intraclasts of clay-rich mudstone. The basement rocks are comprised of metasedimentary rocks, orthogneiss, and lenses and dykes of granitic pegmatite.

The Phoenix deposit is a typical unconformity-related U deposit lying along the unconformity between the Athabasca Group sandstone and the basement rocks (Fig. 2b). The deposit contains several ore pods along northeast striking WS Fault (Fig. 2b). The high-grade cores of the ore pods are surrounded by lower grade margins. A minor volume of the

deposit extends along the WS Fault from the unconformity to the basement (Fig. 2c).

The major structural feature of the Phoenix deposit is the WS Fault along graphitic pelitic gneiss and non-graphitic garnet gneiss (Fig. 2b). The fault is near the western edge of a quartzite ridge that appears to have acted as a resistant block buttress with the strain being accommodated in the pelitic rocks (Kerr 2010). The principal stress responsible for the fault was directed northwest-southeast, and a change in the principal stress to an east-west direction led to later strike-slip movement along the WS Fault (Kerr 2010). The vertical displacement of the unconformity and splay structures of the fault in sandstones support reactivation of the WS Fault during and after the deposition of sandstones.

The sandstones in the study area retain the original depositional texture except for intensely altered rocks near the deposit and the unconformity. The hydrothermal alteration varies in space, and it includes the desilicification (dissolution of silica cement), dravitation, chlorization, kaolinitization, and illitization. The alteration in sandstones appears intense along the splay structures propagating upward from the WS Fault in the basement (Fig. 2b; Roscoe 2015).

Sandstones and whole-rock lithochemical database

The data set for sandstones above the Phoenix deposit contains 4625 samples from 141 drill cores. The drill hole collar locations of these sandstones are within 1 km from the surface projection of the Phoenix deposit (Fig. 2c) and listed in ESM Table 1. Among the samples, 315 are from the MFd, 1416 from the MFc, 944 from the MFb, and 1950 from the RD. Since the MFd is the thinnest unit, it has a smaller number of sandstone data than other units. The drilling was conducted between 2008 and 2011, and the inclinations of the drill holes are vertical to near vertical ($>80^\circ$). Samples for geochemical analysis were collected at approximately 10-m intervals of the entire drill core shortly after the drilling. Samples from the RD near the deposit were collected at 5-m intervals. All lithochemical analyses were conducted at the Saskatchewan Research Council (SRC) for Denison Mines Corp. using the same analytical procedure (code 3AMS). The analysis involved the near-total digestion of rock pulps using a mixture of concentrated HF, HNO₃, and HCl followed by the concentration measurements with inductively coupled plasma optical emission spectrometry (ICP-OES) and inductively coupled plasma mass spectrometry (ICP-MS). Boron was analyzed by ICP-OES after fusion of rock pulps with a mixture of Na₂O₂ and NaCO₃. Details on the analysis method and the quality control procedures are provided by Roscoe (2015). Total Fe contents are expressed as Fe₂O₃ (T).

The lithochemical data contains the abundances of Al₂O₃, Ag, B, Ba, Be, CaO, Co, Cd, Ce, Cr, Cu, Dy, Er, Eu, Fe₂O₃, Ga, Gd, Hf, Ho, K₂O, La, Li, MgO, MnO, Mo, Na₂O,

Nb, Nd, Ni, P₂O₅, Pb, Pr, Sc, Sm, Sn, Sr, Ta, Tb, Th, TiO₂, U, V, W, Y, Yb, Zn, and Zr. In this study, light rare earth elements (LREEs) include La, Ce, Nd, Sm, Eu, and Gd, and heavy REEs (HREEs) are represented by Dy, Er, Ho, and Yb. Note that Si was lost during acid digestion as gaseous SiF₄ and SiO₂ were not determined. The geochemical data used for this study are reported in Dann et al. (2014).

For comparison, we use lithochemical data of sandstones from non-mineralized areas of the eastern Athabasca Basin, east of the Cable Bay Shear Zone (Fig. 1), compiled by Wright et al. (2015) based on Saskatchewan Government assessment records. The total is 336 samples including 9 from the RD, 106 from the MFb, 121 from the MFc, 57 from the MFd, and 43 from the MFr (Raibl Member) and MFw (Warnes Member).

Statistical analysis methodology

The statistical summary of lithochemistry of sandstones overlying Phoenix deposit and sandstones in non-mineralized areas of the eastern Athabasca Basin is provided in ESM Table 2. The raw data were examined before PCA. Firstly, elements that show values below or equal to the detection limits in $>95\%$ samples were removed. They are Ag, Co, Mo, Sc, Sn, Ta, Tb, and W. Among the remaining data, values lower than the detection limits and missing values were replaced using “robCompositions” package by Templ et al. (2010) of the R program (R Core Team 2013). In this study, samples with missing values were less than 5% of the total number of samples, and missing values for Y, REEs, and U are less than 1% of the total. Therefore, any potential bias related to imputed values is considered to be insignificant compared to the geochemical patterns reported in this study. A training set with no censored values was used to estimate replacements for censored values based on a nearest neighbor approach (Hron et al. 2010).

Compositional data of rocks are considered to be “closed” because the sum of analytical data is constant (i.e., 100%), and this “closure” issue results in a lack of independence between variables. To avoid this problem, a centered log ratio transformation was applied to all data prior to statistical analysis as suggested by Aitchison (1986).

Principal component analysis

PCA is a multivariate statistical analysis method that computes eigenvectors, or artificial linear combinations of the original variable (elements), to evaluate the variance of the data set using a small number of orthogonal variables (principal components). Each successive principal component accounts for a lesser and decreasing amount of variance. In geochemical data, most variability is accounted by the first few principal components, thus reducing the number of

dimensions. Each principal component likely reflects an individual process affecting the data, such as alteration and mineralization (Grunsky 2010). PCA has been applied to lithogeochemical data from areas hosting mineral deposits to characterize mineralizing hydrothermal systems (Grunsky 1997; Harris et al. 1997; Chandrajith et al. 2001; Cheng et al. 2011; Chen et al. 2016). RQ-mode PCA is advantageous as it calculates variables and object loadings (variables = elements; objects = samples) on the same axes, so that elements can be displayed along with data points on a single diagram. This study applies RQ-mode PCA to the lithogeochemical data of sandstones overlying the Phoenix deposit (shown in Fig. 2c) to identify elements associated with U.

This study used RQ-mode PCA scripts developed by Grunsky (2001) in the R statistical software environment (R Core Team 2013). The Relative and Absolute Contributions of the elements are calculated after PCA. The Relative Contribution is the contribution of a variable to all the components, and the Absolute Contribution is the contribution of a variable within a given component. The detailed calculation of Relative and Absolute Contributions are described in Grunsky (2010) and Chen et al. (2016).

Element distribution in pseudo-3D

The distribution of the abundances of the elements positively and inversely associated with U was examined in 3D space using the Leapfrog™ modeling software. The concentrations are plotted based on their coordinates of the drill hole collars and depth and projected from a limited distance onto a single 2D cross section. The location of the cross section was select-

ed through the longest axis through the densely populated elongated ellipse of drill cores (Fig. 2c).

Results

PCA

The results of PCA, including eigenvalues, R loadings, Relative and Absolute Contributions, are listed in ESM Table 3. In biplots of PCs, sandstones with relatively high contents of a given element plot close to the position of the element and elements with coherent behavior plot in close proximity to each other. PC1 and PC2 account for 40.2% of the total variation of the data. Scores of samples and variables show distinct groupings of elements (Fig. 3). Relative enrichment of U + HREEs + Y + Pb is shown along the positive PC1 axis in RD, MFc, and MFd units. Relative enrichment of LREE plots exclusively in the RD, along the positive PC1 and PC2 axes (Fig. 3).

PC1 accounts for 41.4% of variability of U concentration (ESM Table 3c). The enrichment of U and REEs is positively associated with Pb + Na + B + Mg + Ni and inversely associated with Fe + Mn + Th + Zr + Hf + Ti + Al + K in PC1 (Fig. 3). Elements V, Cd, Ba, Cr, Zn, and Li have small variability in both PC1 and PC2 (Fig. 3). The scores of PC1 vary among different sandstone units (Fig. 3a) with overall high scores in the RD and moderately positive scores in the MFd (Fig. 3a). The score of U is close to 0 in PC2, indicating that PC2 does not contain much information related to U. Furthermore, the Relative Contributions of U in other PCs are smaller (<11.6%) than that of PC1, suggesting that the variability of U in other PCs is insignificant (ESM Table 3c). Processes responsible for

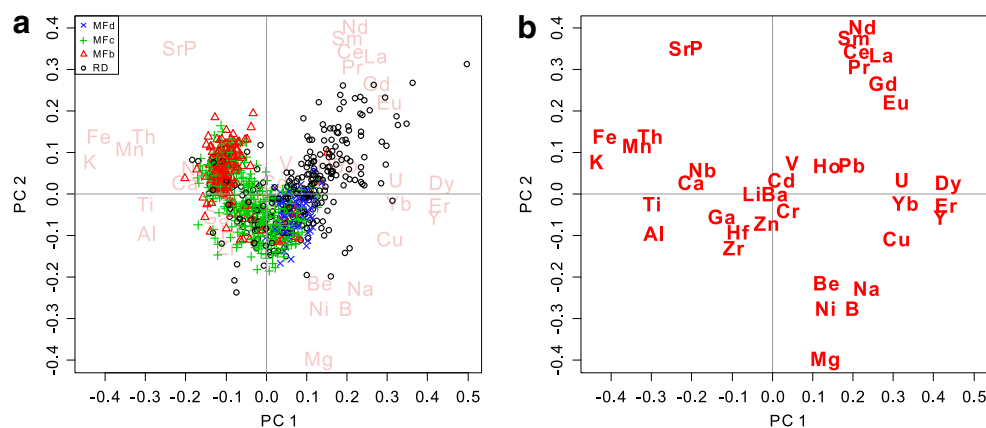


Fig. 3 Biplots of PC1 versus PC2 for the sandstone lithogeochemical data set. For clarity, elements are shown in a faded font in **a** and are shown separately in **b**. Each data point represents one sample. The R loadings are

scaled by a factor of 0.5 for better visualization of elements. Note that the samples from the RD and MFd plot on the positive side of PC1, whereas those of the MFb and MFc are on the negative side of PC1

other PCs had minor effects on the distribution of U. For example, PC8 accounts for only 2.9% of the total variability of the data set (ESM Table 3a) and 0.3% of the variability of U (ESM Table 3c). The process reflected by PC8 did not have significant effects on the distribution of U.

Element distributions

The concentrations of elements positively and inversely associated with U show significant spatial variations in sandstones. Distribution of selected elements associated with U, such as HREEs + Y, B, MgO, and Fe₂O₃ (T), is presented below, and that for U, Pb, Cu, and Th is shown in ESM Figs. 1, 2, 3, and 4.

HREEs and Y

The concentrations of HREEs and Y in sandstones overlying the Phoenix deposit are high relative to those in non-

mineralized sandstones from the eastern part of the Athabasca Basin (Fig. 4a). Sandstones in the RD contain overall higher concentrations of HREEs and Y than those in the upper units (Fig. 4b). Within the study area, sandstones show vertical and spatial variations in their concentrations (Fig. 4b, c). Sandstones directly above the Phoenix deposit, in drill holes within 30 m from the deposit on the plan view, contain relatively high HREEs and Y, with the sum greater than 14 ppm, which is the 90th percentile of the entire data set (Fig. 4c). The maximum value for the combined concentrations of HREEs plus Y is 372 ppm in the RD directly above the deposit (WR-272 at 320 m depth; Fig. 4c). On the other hand, most sandstones in drill cores greater than 200 m from the deposit on the plan view contain low concentrations of Y and HREEs, ranging from 0.2 to 0.5 ppm in total (Fig. 4c). The spatial variation in their concentrations forms a “chimney-like” distribution on the vertical section (Fig. 4c) from the deposit to the uppermost sandstones, as first reported by Dann et al. (2014).

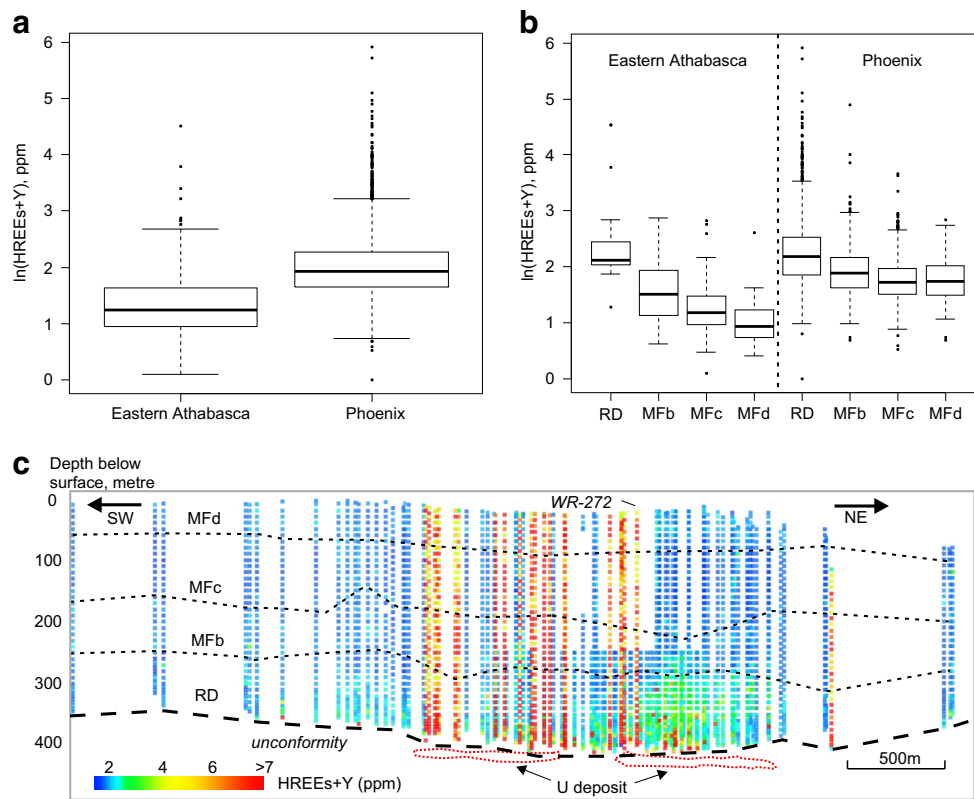


Fig. 4 a Box-and-whisker plots of (HREEs + Y) concentrations of the RD, MFb, MFc, and MFd above Phoenix U deposit and in the eastern Athabasca Basin. Regional sandstone data from the eastern Athabasca Basin compilation of Wright et al. (2015) (*Eastern Athabasca*); sandstone data above the Phoenix U deposit (*Phoenix*). b Box-and-whisker plots of (HREEs + Y) concentrations in the RD and MF sandstones above the

Phoenix U deposit and from the eastern Athabasca Basin. c Spatial distribution of the (HREEs + Y) concentrations. The sample locations are projected on a plane along the strike of the ore bodies (Fig. 2c). Each square on the plot represents one drill core sample. The data are not continuously plotted because of missing data (see text). Vertical exaggeration is 2×. UTM NAD 83 Zone 13 N eastings and northings are in meters

Fig. 5 **a** Box-and-whisker plots of B concentrations in the RD, MFb, MFc, and MFd above the Phoenix U deposit. **b** Spatial distribution of the B concentrations. Plot was constructed in the same way as Fig. 4c

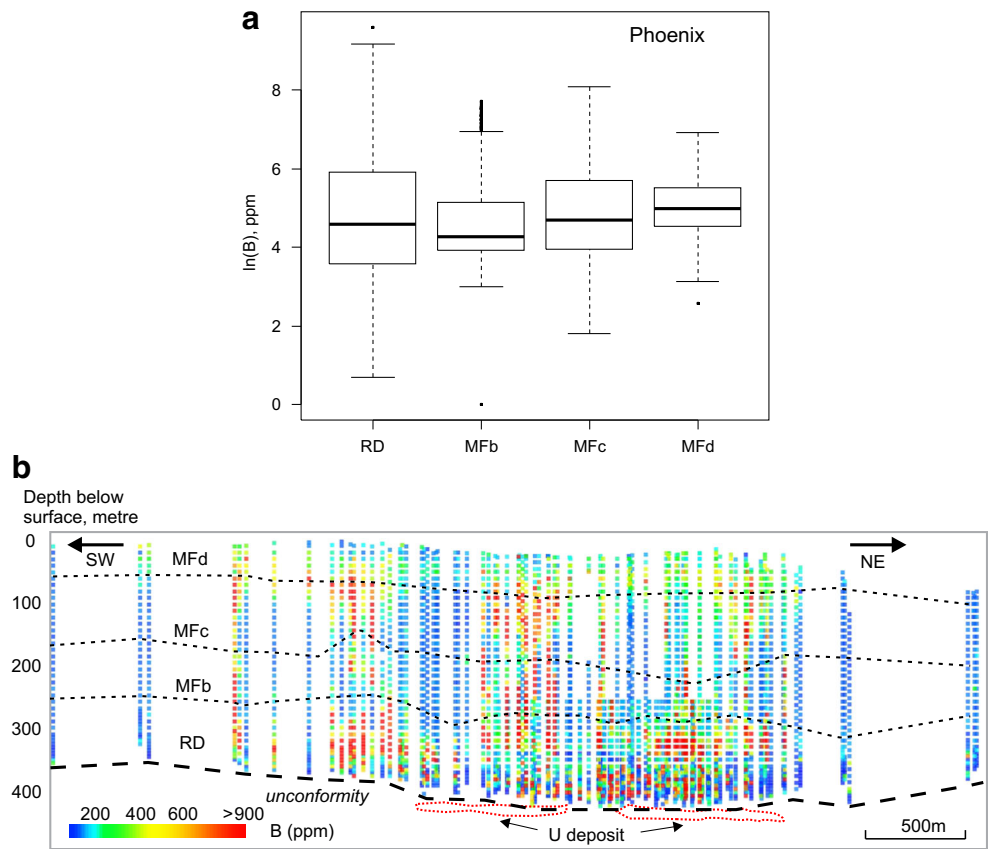
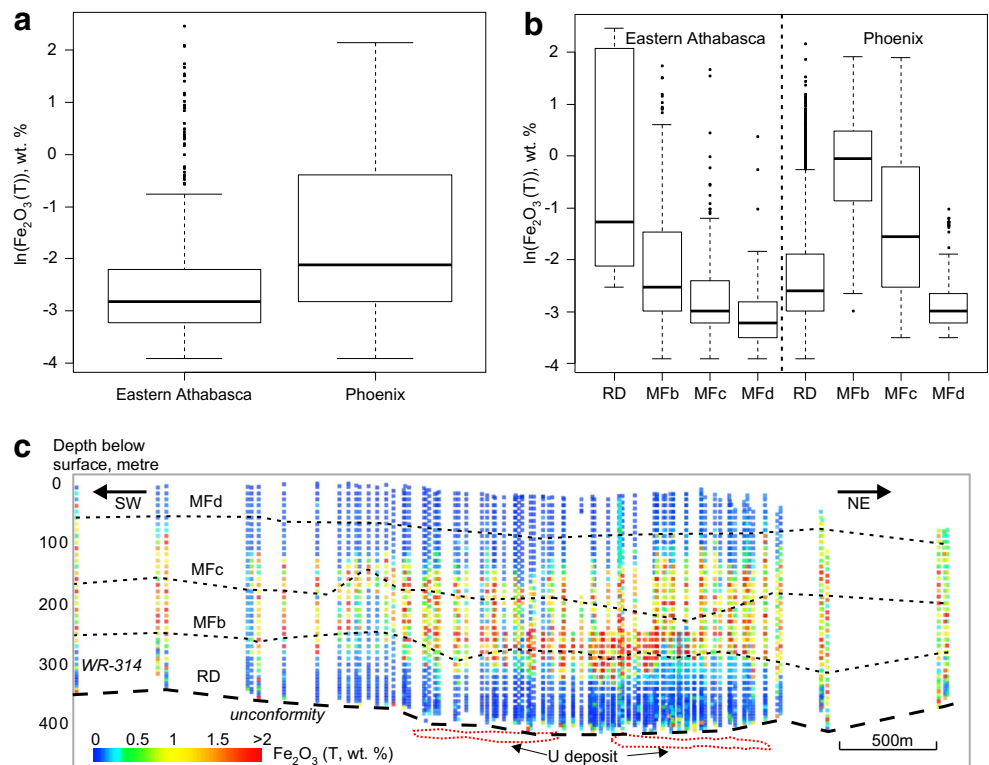


Fig. 6 **a** Box-and-whisker plots of Fe_2O_3 (T) concentrations in the RD and MF sandstones above the Phoenix deposit and the east Athabasca Basin. **b** Box-and-whisker plots of Fe_2O_3 (T) concentrations in the RD, MFb, MFc, and MFd of the Phoenix area and in the eastern Athabasca Basin. **c** Spatial distribution of the total Fe concentrations, reported as Fe_2O_3 (T). Plot was constructed in the same way as Fig. 4c



Boron

High concentrations of B are observed in sandstones of the RD, greater than 286 ppm, the upper quartile value of the Phoenix data set (Fig. 5a, b). Many samples of the MFb and the lower part of the MFc contain B concentration lower than 98 ppm, the median value of the entire Phoenix data set (Fig. 5a, b). The spatial distribution of B abundances shows also a chimney-like pattern above the Phoenix U deposit (Fig. 5b), although it is not as well defined as for that of (HREEs + Y) in Fig. 4c.

Fe₂O₃ (T)

The Fe contents of sandstones above the Phoenix deposit are comparable to those of sandstones in the eastern Athabasca Basin (Fig. 6a), but the values show a distinct variation depending on the stratigraphic units (Fig. 6b). Most sandstones of the MFb and lower MFc contain high Fe₂O₃ (T), greater than 1.5 wt%, the 90th percentile value of the entire Phoenix data set (Fig. 6c). On the other hand, RD and MFd sandstones show generally moderate and low values compared to MFb and MFc sandstones (Fig. 6b, c). Most of the values are less than 0.68 wt%, which is the upper quartile of the entire Phoenix sandstone data set.

MgO

The concentrations of MgO in sandstones above the Phoenix deposit are much higher than those from the eastern Athabasca Basin reported by Wright et al. (2015) (Fig. 7a, b). In the research area, MgO concentrations are high in the RD, MFd, and the upper part of the MFc compared to those of the MFb and the lower part of MFc (Fig. 7c). The elevated MgO contents are also observed in the lower MFb directly above the deposit, which results in a weak chimney-like or “hump-like” pattern of its abundances directly above the deposit (Fig. 7c). In the distal sandstones in drill holes which are over 200 m from the surface projection of ore show high MgO values only in the RD (Fig. 7c).

Lead isotope compositions

The values of ²⁰⁶Pb/²⁰⁴Pb for sandstones overlying the Phoenix deposit are higher than those of barren areas in the eastern Athabasca Basin (Fig. 8a), especially for the RD sandstones (Fig. 8b). ²⁰⁶Pb is a decay product of ²³⁸U with a long half life of 4.5 Ga. Since Pb is mobile at relatively low temperatures, Pb with high radiogenic isotope compositions is commonly attributed to its dispersion from U deposits long time after the mineralization (Holk et al. 2003). However, in situ decay of U in high U/Pb rocks also results in high radiogenic

Fig. 7 **a** Box-and-whisker plots of MgO concentrations in the RD and MF sandstones above the Phoenix U deposit and in the eastern Athabasca Basin. **b** Box plots of MgO concentrations in the RD, MFb, MFc, and MFd above the Phoenix U deposit and in the eastern Athabasca Basin. **c** Spatial distribution of the MgO concentrations. Plot was constructed in the same way as Fig. 4c

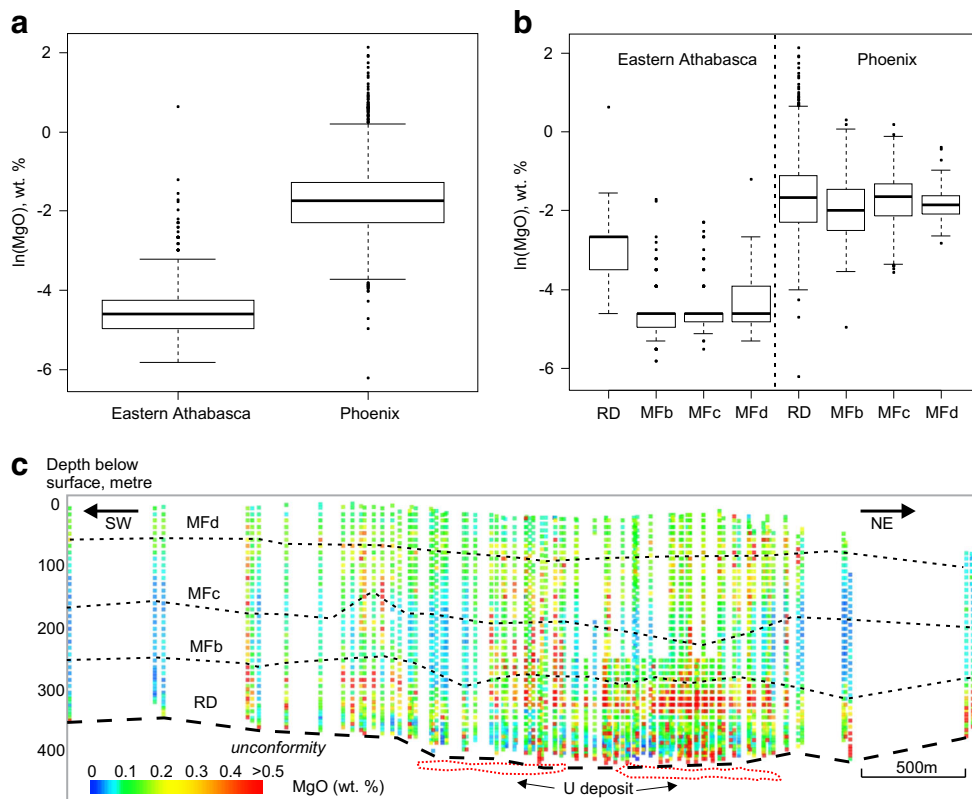
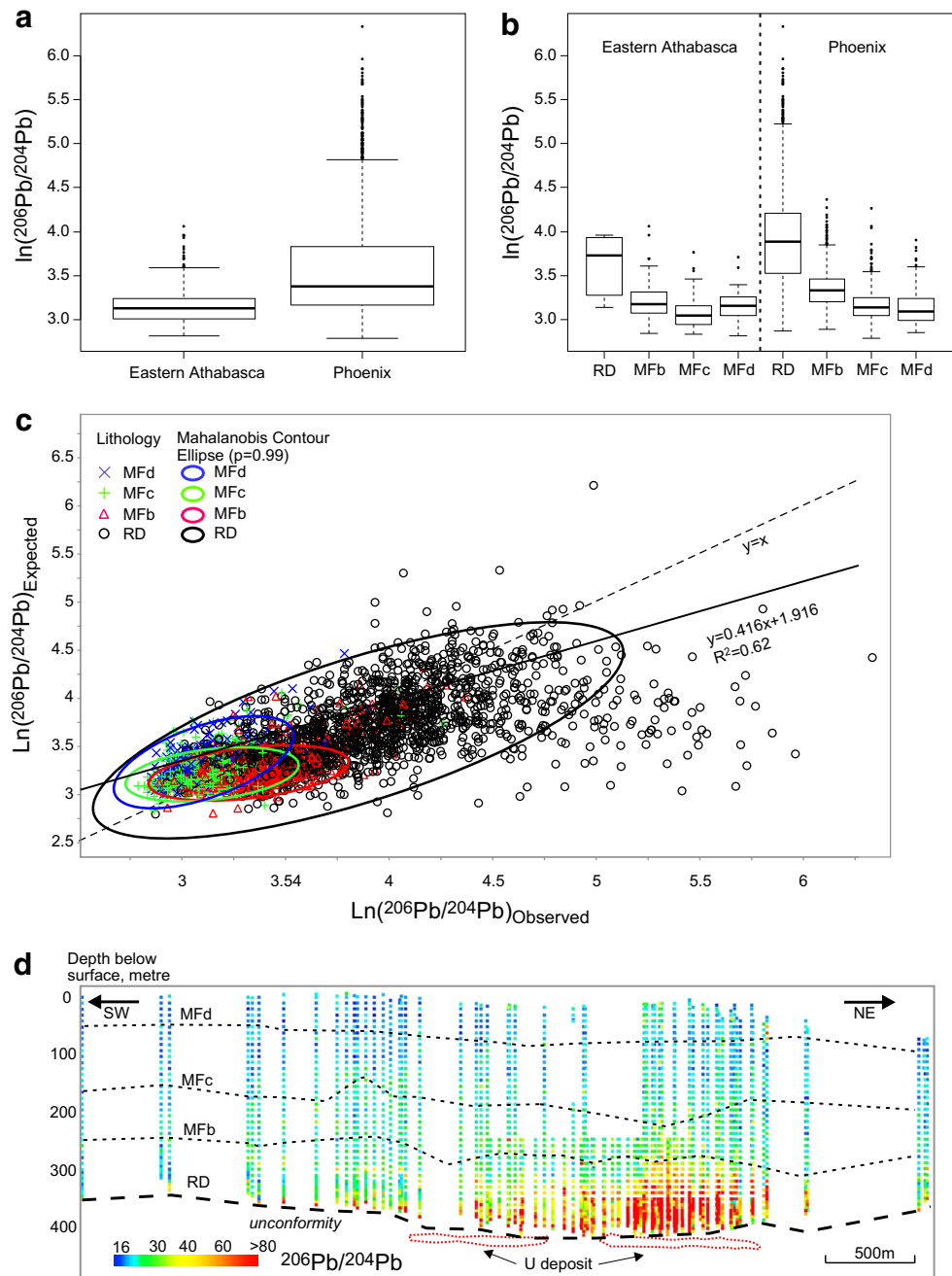


Fig. 8 **a** Box-and-whisker plots of $^{206}\text{Pb}/^{204}\text{Pb}$ values of the RD and MF sandstones above the Phoenix U deposit and in the eastern Athabasca Basin. **b** Box-and-whisker plots of the $^{206}\text{Pb}/^{204}\text{Pb}$ ratios in the Rd., MFb, MFc, and MFd sandstones above the Phoenix U deposit and in the eastern Athabasca Basin. **c** Expected and observed values of $^{206}\text{Pb}/^{204}\text{Pb}$ in natural logarithmic scale. The regression equation was obtained using a robust method described by Leroy and Rousseuw (1987). The Mahalanobis ellipse ($p = 0.99$) represents the 99th quantile of the chi-squared distribution. A significant number of RD sandstones are outside the ellipse and have higher observed $^{206}\text{Pb}/^{204}\text{Pb}$ values than expected. **d** Spatial distribution of $^{206}\text{Pb}/^{204}\text{Pb}$ ratio values. Plot was constructed in the same way as Fig. 4c



Pb isotope compositions. In order to evaluate the source of Pb in sandstones, expected Pb isotope compositions are calculated from the concentrations of U, Th, and crustal average Pb isotope composition at 1.5 Ga using Stacey and Kramers (1975). The observed values of $^{206}\text{Pb}/^{204}\text{Pb}$ are similar to the expected values in most samples, and the two are positively correlated (correlation coefficient (r) = 0.79, Fig. 8c) at a high confidence

level (99%, $p < 0.0001$). This suggests that the observed $^{206}\text{Pb}/^{204}\text{Pb}$ values are the results of in situ decay of U in most sandstones.

^{208}Pb is a decay product of ^{232}Th . The observed and expected values of $^{206}\text{Pb}/^{204}\text{Pb}$ in sandstones are similar except for the RD sandstones close to the Phoenix deposit (ESM Fig. 5). The two are positively correlated ($r = 0.95$) at a high

confidence level (99%, $p < 0.0001$, ESM Fig. 5), supporting that Pb isotope compositions of sandstones are mostly in situ decays of U and Th.

Several RD and MFb sandstones show that observed $^{206}\text{Pb}/^{204}\text{Pb}$ values are higher than calculated values (Fig. 8c). The disparity of the values suggests either the introduction of radiogenic Pb or the loss of U from these sandstones. Since these samples are close to the U deposit (Fig. 8c, d), we suggest the introduction of radiogenic Pb to the sandstones from the deposit long after the mineralization.

Discussion

Source of elements associated with U

The variance of U abundances is mostly accounted by PC1 (41.4%), in which U is associated with HREE, Y, LREEs, Pb, Mg, B, Cu, Na, and Ni and inversely associated with Ti, Fe, Zr, Hf, Al, K, and Th (Fig. 3). The elements associated with U include Pb, B, Cu, and Na. These elements are usually low in abundances in siliclastic sandstones because they are not abundant in most detrital minerals. Furthermore, REEs and Y are not mobile at low temperatures, suggesting that these elements were likely introduced to sandstones through hydrothermal activity. Therefore, they are named as the “hydrothermal dispersion suite.” Their association with U suggests their introduction to sandstones during the uraniferous hydrothermal activity. On the other hand, elements inversely associated with U are named as the “detrital mineral suite” because all except for K are considered not to be soluble in aqueous fluids and are commonly hosted by detrital minerals.

Minerals hosting the elements associated with U

As the lithogeochemical data reflect the abundances and compositions of minerals, the elemental associations identified by PCA provide the information related to the occurrences of minerals (Grunsky 2010). Zircon is the major host of Zr in siliclastic sedimentary rocks, and it contains high concentrations of Hf and HREEs (Hoskin and Schaltegger 2003). The inverse association of U and HREEs with Zr and Hf indicates that zircon is not the major host of U and HREEs in the sandstones overlying the Phoenix U deposit.

Association of REEs and P in PC2 in all sandstone units suggests the occurrence of REE phosphates, such as APS minerals, monazite, and xenotime. Phosphorus is closely associated with Sr (PC1, PC2; Fig. 3), which supports the occurrence of Sr-bearing APS minerals (goyazite/svanbergite;

Mwenifumbo and Bernius 2007). The MFb and MFc sandstones plot toward Sr and P, not toward the LREE (Fig. 3), but the RD sandstones show a broad array toward the LREE on PC1-PC2 diagram, not toward Sr and P (Fig. 3). The observed differences in compositional variation is consistent with the occurrence of LREE-bearing florencitic APS minerals close to U deposits and Sr-rich goyazitic APS minerals far from the deposits (Gaboreau et al. 2007; Adlakha and Hattori 2015).

The HREEs are associated with U in the sandstone above the Phoenix deposit (Fig. 3), but the absolute concentrations of HREEs are overall low, less than 9 ppm (the 90th percentile of the data set) in most samples. Therefore, HREE-bearing minerals have not been identified. With the weak association of P to the (HREEs + Y) in PC2 (Fig. 3), xenotime is the most likely host of U and REEs in the sandstones above the Phoenix deposit. Xenotime is the major host of HREEs in brecciated sandstones in the Maw Zone REE deposit (Quirt et al. 1991; Chen et al. 2016), which is 4 km SW from the Phoenix deposit.

The only mineral containing a significant amount of B in sandstones in the study area is dravitic tourmaline, and it occurs as a detrital mineral and an alteration mineral associated with U deposits in the Athabasca Basin (Hoeve and Quirt 1984; Quirt 2003; Rosenberg and Foit 2006; Adlakha and Hattori 2016). High abundance of dravitic tourmaline is reported in the sandstones above the Phoenix deposit by Dann et al. (2014) and Roscoe (2015) based on X-ray diffraction and short-wave near-infrared spectrometry. A detailed study of alteration minerals in the area by O’Connell et al. (2015) showed that the dravitic tourmaline is magnesiofoitite, alkali-deficient Mg tourmaline. Thus, the B concentrations in sandstones reflect the tourmaline contents in the samples. Using the formula of magnesiofoitite, tourmaline contents are calculated for sandstones in drill holes WR-264, WR-256, WR-290, WR-345, and WR-343. The average tourmaline contents are ca. 2 wt% in sandstones directly above the U deposit. The values are consistent with the visual estimate of tourmaline in thin sections.

Sudoite is a Mg-Al di-trioctahedral chlorite and common around U deposits (Hoeve and Quirt 1984; Percival and Kodama 1989). Percival and Kodama (1989) reported the average composition of sudoite near the Cigar Lake U deposit: $[(\text{Al}_{2.86}\text{Mg}_{1.92}\text{Fe}_{0.13})(\text{Si}_{3.30}\text{Al}_{0.70})\text{O}_{10}(\text{OH},\text{F})_8]$. Sudoite with similar composition is reported in the sandstones above the Phoenix deposit (O’Connell et al. 2015). Therefore, dravitic tourmaline and sudoite likely account for the majority of Mg in the sandstone above the Phoenix deposit.

This study shows that Fe is inversely associated with U in PC1 (Fig. 3). Hematite is a common diagenetic mineral in fluvial sandstones. Indeed, hematite is the major host of Fe in the Athabasca sandstones that are mostly of fluvial origin

(Hoeve and Quirt 1984; Jefferson et al. 2007). In the Phoenix deposit area, sandstones near the U deposit are pervasively bleached (buff-colored) due to crystallization of kaolin minerals and dissolution of the Fe oxides. However, a few samples of the lowermost RD sandstones overlying the U deposit display elevated Fe_2O_3 (T), ~1.5 wt% (Fig. 6a). The data appears to support the hypothesis proposed by Ng et al. (2013) where the ascent of Fe^{2+} -rich fluids from the basement reduced U^{6+} in uraniferous hydrothermal fluid to cause precipitation of uraninite.

Processes forming the vertical element distribution patterns

Elements positively associated with U show “chimney-like” or “hump-like” distribution patterns of their concentrations on the vertical section. The best example is the concentrations of HREEs and Y above the Phoenix U deposit (Fig. 4a). The litho-geochemistry of sandstones reflect the abundance and composition of detrital, diagenetic, and hydrothermal alteration minerals. We consider three possible processes for the vertical distributions of elements:

Hypothesis 1: The patterns reflect original lithological differences. Mudstone and clay intraclasts are common in the RD and the MFd (Ramaekers et al. 2007). Mudstones generally contain high concentrations of U (3.7 ppm), B (100 ppm), and Mg (1.5 wt%) than sandstones (0.5 ppm, 35 ppm, and 0.7 wt%, respectively; Condie 1993). Indeed, these elements are relatively high in sandstones in the RD, lower part of the MFd and upper part of the MFc (Figs. 5b and 7c).

Hypothesis 2: The elements associated with U in PCA were dispersed in sandstones during the uraniferous hydrothermal activity.

Hypothesis 3: This involves transport of elements from the deposit long after the mineralization. Since the U deposit contains high concentrations of U and associated elements, groundwater movement may have dispersed these elements from the deposit to overlying sandstones.

Among three hypotheses, the detrital-diagenetic process (hypothesis 1) is discounted as this cannot explain a chimney-like pattern of high concentrations of elements that cross-cuts the stratigraphy.

The third hypothesis is also discounted because HREEs and Y are not considered mobile elements at low temperatures (<~150 °C, Williams-Jones et al. 2012). The transportation of these elements requires hydrothermal fluids (>200 °C). The major U mineralization event is considered to have occurred at around 1.6 Ga (Alexandre et al.

2009). There is no known extensive hydrothermal activity affecting the study area following the U mineralization. Several dykes, including the Mackenzie dykes at 1.27 Ga (LeCheminant and Heaman 1989) and the Moore Lake Complex at 1.11 Ga (French et al. 2002), generated only local fluid movements around the dykes, as documented in the Centennial U deposit area by Reid et al. (2014). Furthermore, the presence of northwesterly trending Mackenzie dykes has only been so far recorded north of the Phoenix deposit, ~7 km away from the study area (Roscoe 2015).

The remaining hypothesis, hydrothermal dispersion, involves the transport of these elements by hydrothermal fluids during the U mineralization. It is widely accepted that Athabasca unconformity-type U deposits formed by mixing of two fluids: oxidizing basinal fluids and reducing basement fluids (Hoeve and Sibbald 1978; Hoeve and Quirt 1984; Wallis et al. 1984). The oxidizing basinal fluids transported U^{6+} and precipitated U along the unconformity upon mixing with reducing fluids supplied through basement faults (Hoeve and Sibbald 1978; Hoeve and Quirt 1987; Jefferson et al. 2007). Basement fluids are considered to have been enriched in REEs and Y (Hoeve and Quirt 1984; Fayek and Kyser 1997; Kyser et al. 2000; Yeo and Potter 2010; Mercadier et al. 2011b; Adlakha and Hattori 2015, 2016). We propose that the chimney-like distribution of the concentrations of HREEs and Y above the deposit formed by the ascent of the basement fluids. Basement fluids introduced through faults to the unconformity likely continued to flow upwards into sandstones after mixing with basinal fluids near the unconformity. Fluid mixing and mineral precipitation through redox reactions are not necessarily balanced in nature. Without complete precipitation of various minerals, the REEs and Y and other elements in the basement fluids were likely dispersed in sandstones to form the chimney-like distribution of these elements. Similarly, uraniferous basinal fluids may not have been totally reduced by basement fluids at the unconformity, and the circulation of the fluids around the deposit likely dispersed elements in the sandstones.

Another line of supporting evidence is related to the Fe contents in the sandstones. The Athabasca sandstones are mostly of fluvial origin. Such post-Archean continental sandstones are almost always red due to the presence of Fe oxides and hydroxides (Pettijohn et al. 1987). The uraniferous fluids are considered to have been oxidizing and moderately acidic (Jefferson et al. 2007; Cuney 2009; Mercadier et al. 2011a; Adlakha and Hattori 2015). The solubility of Fe is pH dependent, and the moderately acidic fluids can dissolve earlier formed diagenetic hematite and Fe(III) oxyhydroxides. Therefore, the uraniferous fluids could have dissolved moderate amounts of Fe in

sandstones. It is also possible that reducing fluids from the basement dissolved Fe oxides to soluble Fe^{2+} . Hoeve and Quirt (1984, 1987) suggested that the ascent of the reducing basement fluid has resulted in bleached haloes surrounding unconformity-type U deposits. The contents of Fe (Fig. 6b, ESM Table 4) in the RD sandstones in eastern Athabasca Basin are higher than those in the RD sandstones overlying Phoenix deposit. The difference in Fe contents of the two areas supports the removal of Fe from sandstones by uraniferous hydrothermal activity in the sandstones overlying Phoenix deposit.

Factors affecting the hydrothermal activity in the study area

The site of the Phoenix U deposit had several favorable conditions for the U mineralization. As fluid flow is primarily controlled by permeability, faults and the unconformity enhance fluid flow. Furthermore, sandstones are permeable compared to the crystalline basement rocks. Therefore, the topography of the unconformity strongly affects fluid flow patterns and the size of hydrothermal convection cells (Hoeve and Quirt 1984; Raffensperger and Garven 1995).

The study area has highly irregular unconformity due to the presence of quartzite ridges (Fig. 2b), and graben-like structures due to offsets of reactivated basement faults. The main quartzite ridge near the Phoenix deposit is over 200 m above the unconformity (Kerr 2010) and is accompanied by talus deposits (Fig. 2b). The breccias in the talus deposits and basal conglomerate beds are common in topographic lows and depressions, and they are permeable to allow fluid circulation. Such rugged topography of the unconformity likely provided

several confined areas to produce convective hydrothermal fluid flows in sandstones. Together with major faults in the basement, the site was likely to be ideal for the mixing of oxidizing basinal fluids and reduced basement fluids to form the U deposit.

Effects of secondary dispersion

As discussed above, hydrothermal dispersion of elements related to uraniferous hydrothermal activity is captured by PC1. Elements positively associated with U show high loadings in PC1, but some elements have also significant loadings in other PCs. For example, Pb shows high Relative Contribution in PC8 (31.1%, ESM Table 3c), indicating that PC8 provides information on the dispersion of Pb. PC8 also accounts for large part of the total variabilities of Ba and Mn (24.3 and 9.4%, ESM Table 3c). Other elements, including U and REEs + Y, do not show significant loadings in PC8 (<6%, ESM Table 3c). This indicates that PC8 reflects the geological process responsible for the dispersion of Pb, Ba, and Mn, but not U, REEs, and Y. Considering that Pb, Ba, and Mn are soluble at low temperatures, it is very likely that PC8 represents the secondary dispersion in the study area. The scores of PC8 are high in the RD sandstones compared to MFb, MFc, and MFd (Fig. 9). This supports the proposed interpretation based on Pb isotope compositions that Pb was likely dispersed from the deposit to the overlying sandstones some time after the mineralization. Based on the low eigenvalue, 1.1, of PC8, we suggest that the secondary dispersion has very minor effects on the overall lithogeochemistry of sandstones.

Summary

The RQ-mode PCA reduces the number of variables and visualizes relationships among elements in the multivariate space. The result of PCA of lithogeochemical data from sandstones above the Phoenix U deposit shows that U is associated with HREEs + Y, LREEs, B, Na, Mg, Pb, Cu, Be, and Ni and is inversely associated with elements common in detrital minerals, such as Ti, Zr, Hf, Th, and Fe. The association of P with REEs suggests that the major hosts of REEs are APS minerals and xenotime. The sandstones of the RD and MFd show high scores of elements associated with U, which suggests the high abundance of alteration minerals compared to other units. On the other hand, the MFb and MFc sandstones contain high concentrations of Ti, Zr,

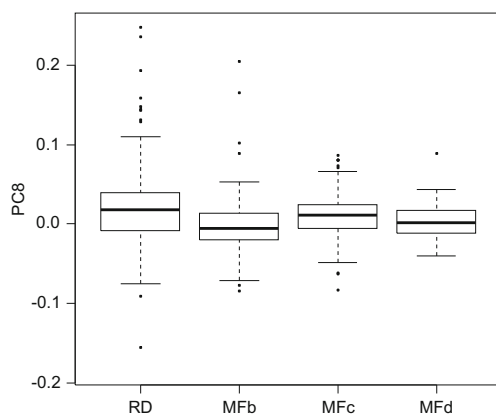


Fig. 9 Box-and-whisker plots of PC8 scores in the sandstones of the RD, MFb, MFc, and MFd above the Phoenix U deposit

Hf, and Th. The suite of elements is high in detrital minerals, which is consistent with the presence of heavy mineral seams in these units. Several elements, such as HREEs and Y, show a chimney-like distribution of their concentrations in sandstones directly above the U deposit. The chimney-like distribution of these elements' abundances is explained by the outflow of basement fluids after mixing with basinal fluids to form the U deposit. The observed Pb isotope compositions are similar to the expected values calculated from the concentrations of U, Th, and Pb in most sandstones except for those close to the U deposit. The data suggest that Pb isotope compositions are explained by in situ decay of U and Th in most sandstones. Radiogenic Pb dispersed from the U deposit to proximal sandstones long after the mineralization. This secondary dispersion of Pb is captured by PC8, which shows high loadings of Pb, Ba, and Mn in the RD sandstones close to the deposit (Fig. 9). PC8 has a small eigenvalue; therefore, the secondary dispersion had a minor effect on the overall lithochemistry of sandstones.

Acknowledgements This study is a part of PhD project by SC at the University of Ottawa. Denison Mines Corp. provided the geochemical data and drill log data to the research team at the University of Ottawa. We thank their logistical support during our field work and approving the publication of this manuscript. Special thanks extend to Lawson Forand (Exploration Manager), Dale Verran (Vice President, Exploration), Chad Sorba, and Yongxing Liu. The research project is funded by a grant to KH from Natural Resources of Canada through the TGI-4 Uranium Ore System program. We thank Sean Bosman of Saskatchewan Geological Survey for clarification of the Athabasca sandstone stratigraphy. We received helpful comments from Julien Mercadier, Donald Wright, and Eric Potter on an earlier draft. Special thanks extend to the Editor-in-Chief, Georges Beaudoin, and the Associate Editor, Mostafa Fayek, and journal reviewers of this manuscript, Charlie Jefferson, Kevin Ansdell, David Quirt, and Antonin Richard. We thank ARANZ Geo Limited for providing an education license of Leapfrog™ 3D geological modeling program.

References

- Adlakha EE, Hattori K (2015) Compositional variation and timing of aluminum phosphate-sulfate minerals in the basement rocks along the P2 fault and in association with the McArthur River uranium deposit, Athabasca Basin, Saskatchewan, Canada. *Am Mineral* 100:1386–1399
- Adlakha EE, Hattori K (2016) Paragenesis and composition of tourmaline types along the P2 fault and McArthur River uranium deposit, Athabasca Basin, Canada. *Can Mineral* 54:661–679
- Aitchison J (1986) *The statistical analysis of compositional data*. Chapman and Hall, London
- Alexandre P, Kyser K, Thomas D, Polito P, Marlat J (2009) Geochronology of unconformity-related uranium deposits in the Athabasca Basin, Saskatchewan, Canada and their integration in the evolution of the basin. *Mineral Deposita* 44:41–59
- Annesley IR, Madore C, Portella P (2005) Geology and thermotectonic evolution of the western margin of the Trans-Hudson Orogen: evidence from the eastern sub-Athabasca basement, Saskatchewan. *Can J Earth Sci* 42:573–597
- Chandrajith R, Dissanayake CB, Tobschall HJ (2001) Application of multi-element relationships in stream sediments to mineral exploration: a case study of Walawe Ganga Basin, Sri Lanka. *Appl Geochem* 16:339–350
- Chen S, Hattori K, Grunsky EC (2016) Multivariate statistical analysis of the REE-mineralization of the Maw Zone, Athabasca Basin, Canada. *J Geochem Explor* 161:98–111
- Cheng Q, Bonham-Carter G, Wang W, Zhang S, Li W, Qinglin X (2011) A spatially weighted principal component analysis for multi-element geochemical data for mapping locations of felsic intrusions in the Gejiu mineral district of Yunnan, China. *Comput Geosci* 37:662–669
- Clark LAC (1987) Near surface lithochemical halos as an aid to discovery of deeply buried unconformity-type deposits, Athabasca Basin, Canada. *J Geochem Explor* 28:71–84
- Condie KC (1993) Chemical composition and evolution of the upper continental crust: contrasting results from surface samples and shales. *Chem Geol* 104:1–37
- Creaser R, Stasiuk L (2007) Depositional age of the Douglas Formation, northern Saskatchewan, determined by Re-Os geochronology. In: Jefferson CW, Delaney G (eds) *EXTECH IV: Geology and Uranium Exploration TECHNOLOGY of the Proterozoic Athabasca Basin, Saskatchewan and Alberta*. Geol Surv Canada, Bull 588, pp 341–346
- Cuney M (2009) The extreme diversity of uranium deposits. *Mineral Deposita* 44:3–9
- Dann J, Hattori K, Potter EG, Sorba C (2014) Discrimination of elemental assemblages in the alteration halo of the Phoenix deposit, Saskatchewan, through applied GIS. *Geol Surv Canada, Open File* 7463
- Earle S, Sopuck V (1989) Regional lithochemistry of the eastern part of the Athabasca Basin uranium province, Saskatchewan. In: Muller-Kahle E (ed) *Uranium Resources and Geology of North America: International Atomic Energy Agency, Technical Document TECDOC-500*, pp 263–269
- Fayek M, Kyser TK (1997) Characterization of multiple fluid events and rare-earth-element mobility associated with formation of unconformity-type uranium deposits in the Athabasca Basin, Saskatchewan. *Can Mineral* 35:627–658
- Filzmoser P, Hron K, Reimann C (2010) The bivariate statistical analysis of environmental (compositional) data. *Sci Total Environ* 408:4230–4238
- French JE, Heaman LM, Chacko T (2002) Feasibility of chemical U–Th–total Pb baddeleyite dating by electron microprobe. *Chem Geol* 188:85–104
- Gaboreau S, Cuney M, Quirt D, Beaufort D, Patrier P, Mathieu R (2007) Significance of aluminum phosphate-sulfate minerals associated with U unconformity-type deposits: the Athabasca Basin, Canada. *Am Mineral* 92:267–280
- Gamelin C, Sorba C, Kerr W (2010) The discovery of the Phoenix deposit: a new high-grade Athabasca Basin unconformity-type

- uranium deposit, Saskatchewan, Canada. In: Sask Geol Surv Open House 2010 Abstract Volume, pp 10
- Grunsky, EC (1997) Strategies and methods for the interpretation of geochemical data. In: Current Topics in GIS and Integration of Exploration Datasets, Short Course, Exploration'97 Workshop, Ottawa, Canada
- Grunsky EC (2001) A program for computing RQ-mode principal components analysis for S-plus and R. *Comput Geosci* 27: 229–235
- Grunsky EC (2010) The interpretation of geochemical survey data. *Geochem-Explor Env A* 10:27–74
- Guffey S, Piercey S, Ansdell K, Kyser K, Kotzer T, Zaluski G (2015) Potential pathfinder elements: footprint of 3D litho-geochemistry of the millennium unconformity-type uranium deposit, Athabasca Basin, Saskatchewan. 27th International Applied Geochemistry Symposium, Tucson, USA, Abstract
- Harris JR, Grunsky EC, Wilkinson L (1997) Developments in the effective use of litho-geochemistry in regional exploration programs: application of GIS technology. In: Gubins AG (ed) Proceedings of the Exploration'97, Fourth Decennial International Conference on Mineral Exploration, pp 285–292
- Hoeve J, Quirt DH (1984) Mineralization and host rock alteration in relation to clay mineral diagenesis and evolution of the middle-Proterozoic Athabasca Basin, northern Saskatchewan, Canada. Sask Res Council Technical Report 187
- Hoeve J, Quirt DH (1987) A stationary redox front as a critical factor in the formation of high-grade unconformity-type uranium ores in the Athabasca Basin, northern Saskatchewan. *Bull Minéral* 110:157–171
- Hoeve J, Sibbald TII (1978) On the genesis of Rabbit Lake and other unconformity-type uranium deposits in northern Saskatchewan, Canada. *Econ Geol* 73:1450–1473
- Holk GJ, Kyser TK, Chipley D, Hiatt EE, Marlatt J (2003) Mobile Pb-isotopes in Proterozoic sedimentary basins as guides for exploration of uranium deposits. *J Geochem Explor* 80:297–320
- Hoskin PWO, Schaltegger U (2003) The composition of zircon and igneous and metamorphic petrogenesis. *Rev Mineral Geochem* 53: 27–53
- Hron K, Templ M, Filzmoser P (2010) Imputation of missing values for compositional data using classical and robust methods. *Comput Stat Data Anal* 54:3095–3107
- Jefferson CW, Thomas DJ, Gandhi SS, Ramaekers P, Delaney G, Brisbin D, Cutts C, Quirt D, Portella P, Olson RA (2007) Unconformity-associated uranium deposits of the Athabasca Basin, Saskatchewan and Alberta. In: Goodfellow WD (ed) Mineral Deposits of Canada: A Synthesis of major deposit-types, district metallogeny, the evolution of geological provinces, and exploration methods, Geological Association of Canada, Mineral Deposits Division, Spec Publ, Vol 5, pp 273–305
- Kerr WC (2010) The discovery of the Phoenix deposit: a new high-grade, Athabasca Basin unconformity-type uranium deposit, Saskatchewan, Canada. *Soc Econ Geol Spec Publ* 15: 703–728
- Kister P, Laverret E, Quirt D, Cuney M, Mas PP, Beaufort D, Bruneton P (2006) Mineralogy and geochemistry of the host-rock alterations associated with the Shea Creek unconformity-type uranium deposits (Athabasca basin, Saskatchewan, Canada). Part 2. Regional-scale spatial distribution of the Athabasca group sandstone matrix minerals. *Clay Clay Miner* 54:295–313
- Kotzer T, Kyser TK (1995) Fluid history of the Athabasca Basin and its relation to diagenesis, uranium mineralization and paleohydrology. *Chem Geol* 120:45–89
- Kyser K, Hiatt E, Renac C, Durocher K, Holk G, Deckart K (2000) Diagenetic fluids in Paleo-and Meso-Proterozoic sedimentary basins and their implications for long protracted fluid histories. Fluids and basin evolution: Mineral Assoc Canada Short Course Series, Vol 28, pp 225–262
- Laverret E, Patrier P, Beaufort D, Kister PH, Quirt D, Bruneton P, Clauer N (2006) Mineralogy and geochemistry of hostrock alterations associated with the Shea Creek unconformity type uranium deposits (Saskatchewan, Canada). Part 1: spatial variation of illite properties. *Clay Clay Miner* 54:275–294
- LeCheminant AN, Heaman LM (1989) Mackenzie igneous events, Canada: middle Proterozoic hotspot magmatism associated with ocean opening. *Earth Planet Sci Lett* 96:38–48
- Leroy AM, Rousseeuw PJ (1987) Robust regression and outlier detection. Wiley Series in Probability and Mathematical Statistics. Wiley, New York
- Lewry JF, Sibbald TII (1980) Thermotectonic evolution of the Churchill province in northern Saskatchewan. *Tectonophysics* 68:45–82
- Li Z, Chi G, Bethune KM, Bosman SA, Card CD (2015) Geometric and hydrodynamic modelling and fluid-structural relationships in the southeastern Athabasca Basin and significance for uranium mineralization. In: Potter EG, Wright DM (eds) Targeted Geoscience Initiative 4: unconformity-related uranium systems. Geol Surv Canada, Open File 7791, pp 103–114
- McGill B, Marlatt J, Matthews R, Sopuck V, Homeniuk L, Hubregtse J (1993) The P2 North uranium deposit Saskatchewan, Canada. *Explor Min Geol* 2:321–331
- McKechnie CL, Annesley IR, Ansdell KM (2012) Medium-to low-pressure pelitic gneisses of Fraser Lakes zone B, Wollaston Domain, northern Saskatchewan, Canada: mineral compositions, metamorphic P-T-t path, and implications for the genesis of radioactive abyssal granitic pegmatites. *Can Mineral* 50:1669–1694
- Mellinger M, Quirt DH, Hoeve J (1987) Geochemical signatures of uranium deposition in the Athabasca Basin of Saskatchewan, Canada. *Uranium* 3:187–209
- Mercadier J, Cuney M, Lach P, Boiron MC, Bonhoure J, Richard A, Leisen M, Kister P (2011a) Origin of uranium deposits revealed by their rare earth element signature. *Terra Nova* 23: 264–269
- Mercadier J, Cuney M, Cathelineau M, Lacorde M (2011b) U redox fronts and kaolinisation in basement-hosted unconformity-related U ores of the Athabasca Basin (Canada): late U remobilisation by meteoric fluids. *Mineral Deposita* 46:105–135
- Mwenifumbo CJ, Bernius GR (2007) Crandallite-group minerals: host of thorium enrichment in the eastern Athabasca basin, Saskatchewan. In: Jefferson CW and Delaney G (eds) EXTECH IV: Geology and Uranium Exploration TECHNOLOGY of the Proterozoic Athabasca Basin, Saskatchewan and Alberta. Geol Surv Canada, Bull 588, pp 521–638
- Ng R, Alexandre P, Kyser K (2013) Mineralogical and geochemical evolution of the unconformity-related McArthur River zone 4 orebody in the Athabasca Basin, Canada: implications of a silicified zone. *Econ Geol* 108:1657–1689
- O'Connell I, Hattori K, Chen S, Adlakha EE, Sorba C (2015) Characterization of tourmaline from the Maw Zone, gryphon zone and sandstones above the Phoenix uranium deposits, Athabasca

- Basin, Saskatchewan, Canada. Geol Surv Canada, Scientific Presentation 37
- Percival JB, Kodama H (1989) Sudoite from Cigar Lake, Saskatchewan. *Can Mineral* 27:633–641
- Pettijohn FJ, Potter PE, Siever R (1987) Sand and sandstone. Springer-Verlag, Berlin
- Quirt DH (2003) Athabasca unconformity-type uranium deposits: one deposit type with many variations. In: Cuney M (ed) Proceedings of Uranium Geochemistry 2003 International Conference, pp 309–312
- Quirt DH, Wasyluk K (1997) Kaolinite, dickite, and other clay minerals in the Athabasca Group, Canada, and the Kombolgie Formation, Australia. 11th International Clay Conference, Ottawa, Canada, Abstract A61
- Quirt DH, Kotzer T, Kyser K (1991) Tourmaline, phosphate minerals, zircon, and pitchblende in the Athabasca Group: Maw Zone and McArthur River areas, Saskatchewan. In: Summary of Investigations 1991, Sask Geol Surv, Sask Energy and Mines, Misc Rep 91-4, pp 181–191
- R Core Team (2013) R: A language and environment for statistical computing. R Foundation for Statistical Computing, Vienna, Austria. <http://www.R-project.org/>
- Raffensperger JP, Garven G (1995) The formation of unconformity-type uranium ore deposits; 1, coupled groundwater flow and heat transport modeling. *Am J Sci* 295:581–636
- Ramaekers P, Jefferson CW, Yeo, GM, Collier B, Long DGF, Drever G, Wheatley K (2007) Revised geological map and stratigraphy of the Athabasca Group, Saskatchewan and Alberta. In: Jefferson CW and Delaney G (eds) EXTECH IV: Geology and Uranium Exploration TECHNOLOGY of the Proterozoic Athabasca Basin, Saskatchewan and Alberta. Geol Surv Canada, Bull 588, pp 155–190
- Reid KD, Ansdell K, Jiricka D, Witt G, Card C (2014) Regional setting, geology, and paragenesis of the centennial unconformity-related uranium deposit, Athabasca Basin, Saskatchewan, Canada. *Econ Geol* 109:539–566
- Roscoe W (2015) Technical report on a mineral resource estimate update for the Phoenix uranium deposit, Wheeler River Project, eastern Athabasca Basin, northern Saskatchewan, Canada. NI 43-101 Report
- Rosenberg PE, Foit FF (2006) Magnesiofoitite from the uranium deposits of the Athabasca Basin, Saskatchewan, Canada. *Can Mineral* 44: 959–965
- Sopuck VJ, de Carle EM, Cooper B (1983) The application of lithochemistry in the search for unconformity-type uranium deposits, northern Saskatchewan, Canada. *J Geochem Explor* 19:77–99
- Stacey JT, Kramers JD (1975) Approximation of terrestrial lead isotope evolution by a two-stage model. *Earth Planet Sci Lett* 26:207–221
- Templ M, Hron K, Filzmoser P (2010) robCompositions: Robust estimation for compositional data. Manual and package, version 1.3.3
- Wallis RH, Saracoglu N, Golightly JP, Brummer JJ (1984) Geology of the McClean uranium deposits, northern Saskatchewan. *CIM (Can Inst Min Metall) Bull* 77:69–96
- Williams-Jones AE, Migdisov AA, Samson IM (2012) Hydrothermal mobilization of the rare earth elements—a tale of “ceria” and “yttria”. *Elements* 8:355–360
- Wright DM, Potter EG, Comeau JS (2015) Athabasca Basin Uranium Geochemistry Database v.2. Geol Surv Canada, Open File 7792
- Yeo G, Delaney G (2007) The Wollaston Supergroup, stratigraphy and metallogeny of a Paleoproterozoic Wilson Cycle in the Trans-Hudson Orogen, Saskatchewan. In: Jefferson CW and Delaney G (eds) EXTECH IV: Geology and Uranium Exploration TECHNOLOGY of the Proterozoic Athabasca Basin, Saskatchewan and Alberta. Geol Surv Canada, Bull 588, pp 89–117
- Yeo G, Potter E (2010) Review of reducing mechanisms potentially involved in the formation of unconformity-type uranium deposits and their relevance to exploration. In Summary of Investigations, Volume 2, Sask Geol Surv, Sask Ministry of Energy and Resources, Misc Rep, Report 2010–4.2, Paper A-12